Inorganic Chemistry

Article

pubs.acs.org/IC

Solid-State NMR Study of Li-Assisted Dehydrogenation of Ammonia Borane

Takeshi Kobayashi,[†] Ihor Z. Hlova,[†,‡] Niraj K. Singh,[†] Vitalij. K. Pecharsky,[†,‡] and Marek Pruski*[,†,§]

[†]U.S. DOE Ames Laboratory, [‡]Department of Materials Science and Engineering, and [§]Department of Chemistry, Iowa State University, Ames, Iowa 50011, United States

Supporting Information

ABSTRACT: The mechanism of thermochemical dehydrogenation of the 1:3 mixture of Li_3AlH_6 and NH_3BH_3 (AB) has been studied by the extensive use of solid-state NMR spectroscopy and theoretical calculations. The activation energy for the dehydrogenation is estimated to be 110 kJ mol^{-1}, which is lower than for pristine AB (184 kJ mol^{-1}). The major hydrogen release from the mixture occurs at 60 and 72 °C, which compares favorably with pristine AB and related hydrogen storage materials, such as lithium amidoborane ($LiNH_2BH_3$, LiAB). The NMR studies suggest that Li_3AlH_6 improves the dehydrogenation kinetics of AB by forming an intermediate compound $(LiAB)_x(AB)_{1-x}$. A part of AB in the mixture transforms into LiAB to form this intermediate, which accelerates the subsequent formation of branched polyaminoborane species and further release of hydrogen. The detailed reaction mechanism, in particular the role of lithium, revealed in the present study highlights new opportunities for using ammonia borane and its derivatives as hydrogen storage materials.

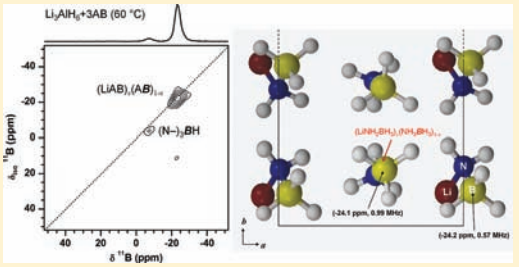

1. INTRODUCTION

Limited reserves of fossil fuels and the environmental impacts resulting from the ever-growing rates of their combustion have increased the demand for alternative sources of energy. Hydrogen is being considered as one of the best alternative fuels (in spite of being an energy carrier rather than a primary energy source), mainly because of the abundance, high gravimetric energy density, and environmental friendliness.[1,2] However, the technical challenges associated with production of hydrogen and its safe and convenient storage and delivery hinder its broad use as an energy carrier.[3,4] To overcome these difficulties several hydrogen storage routes have been examined, the most promising being in solid materials.[5−10] Typical examples of such materials are microporous media,[5,10] intermetallic hydrides,[6] metal nitrides and imides,[9] as well as a number of complex hydrides.[7,8]

Among various hydrides, ammonia borane (NH_3BH_3, henceforth referred to as AB) has attracted considerable attention in recent years.[11−31] AB is a white crystalline solid, whose hydrogen content (19.6 wt %) exceeds by a factor of more than two the 9.0 wt % target set by the U.S. Department of Energy for 2015.[1] Pristine AB is stable at ambient temperature; however, two-thirds of available hydrogen is released upon thermolysis at moderate temperature (<200 °C) via a two-step decomposition to polyaminoborane ($[NH_2BH_2]_n$) and polyiminoborane ($[NHBH]_n$), with both transformations being accompanied with hydrogen release. In addition to hydrogen, volatile gaseous byproducts like borazine ($N_3B_3H_6$) and diborane (B_2H_6) are also produced during these transformations.[19,27] Above 500 °C, the remaining one-third of hydrogen is liberated when $[NHBH]_n$ decomposes to boron nitride (BN) and hydrogen.[19]

Despite the high hydrogen content, practical application of AB as an on-board hydrogen source suffers from sluggish dehydrogenation kinetics at moderate temperatures, concurrent emission of borazine and diborane, and the absence of effective methods for regeneration of spent AB.[16,27,32] Several approaches have been tried in pursuit of improving the dehydrogenation properties of AB and inhibiting the emission of volatile (and poisonous, B_2H_6) gases. Thus, Gutowska et al.[11] reported that the thermolysis of AB on mesoporous silica (SBA-15) exhibits improved dehydrogenation kinetics with suppression of the volatile gaseous products. Denney et al.[12] and Keaton et al.[13] found that the hydrogen release from AB in nonaqueous solutions can be promoted by the transition metal based catalysts. Sneddon et al.[33] reported the acceleration of dehydrogenation from AB in an ionic solution by alkali metal. Yan et al.[14] and Chandra et al.[15] reported that catalysts can improve the dehydrogenation kinetics of AB in aqueous solution as well. The study of Cheng et al.[17] showed that the submicrometer-size $Ni_{1-x}Pt_x$ hollow spheres exhibit favorable catalytic activities in both hydrolysis and thermolysis of AB. The catalytic effect of nanosized Co and Ni on the dehydrogenation properties of AB was reported by He et al.[25] Furthermore, a number of chemical additives such as diammoniate of diborane,[22] BN nanoparticles,[34] transition metal chlorides,[26] and various metal hydrides and amides[19,20,27,35−37] have been reported to exhibit catalytic

Received: November 1, 2011
Published: March 21, 2012

effects in the dehydrogenation of AB. In particular, chemical modifications through reaction of AB with different metal hydrides have produced several metal amidoboranes that exhibit high hydrogen capacity and improved dehydrogenation kinetics along with the suppression of volatile gases.[19,20,35,36]

In the present work, we studied the thermal decomposition of the 1:3 mixture of Li_3AlH_6 and AB (henceforth Li_3AlH_6-3AB) using solid-state NMR spectroscopy (SSNMR) and theoretical calculations. The diagnostic power of SSNMR relies on its ability to probe the structural details of both crystalline and amorphous phases of complex hydride materials in a quantitative manner. Indeed, SSNMR measurements have been widely used for studying the chemical transformation of several classes of metal hydrides, including AB and related compounds.[5,19,20,27,30,38−41] The development of sophisticated computational methods has enabled the use of theory to corroborate the NMR results and refine the structural information.[42]

On the basis of the reported chemical reaction between lithium hydride (LiH) and AB,[19,35] we expected that the thermal treatment of Li_3AlH_6-3AB may proceed via the formation of lithium amidoborane ($LiNH_2BH_3$; LiAB) through the reaction $Li_3AlH_6 + 3AB = 3LiAB + Al + 9/2\ H_2$. However, the SSNMR measurements and theoretical calculations suggest that thermal decomposition of the mixture under investigation proceeds via the formation of a different intermediate phase, leading to improved dehydrogenation properties as compared to pristine AB.

2. EXPERIMENTAL SECTION

2.1. Sample Preparations. Li_3AlH_6 was synthesized by ball milling of the 1:2 molar mixture of $LiAlH_4$ (≥97 wt % purity, Alfa Aesar) and LiH (≥95 wt % purity, Sigma Aldrich).[43] A reference sample of LiAB was synthesized by ball milling of the 1:1 molar mixture of LiH and AB (≥97 wt % purity, Sigma-Aldrich) at −15 °C.[19] Phase purities of the synthesized Li_3AlH_6 and LiAB were confirmed by powder X-ray diffraction (see Supporting Information for details). Because of air sensitivity of the starting materials and the products, all manipulations with the samples were carried out under a continuously purified and monitored argon atmosphere in a glovebox. The Li_3AlH_6-3AB samples studied throughout this work were thoroughly mixed by hand-grinding in a mortar with a pestle for 5 min. The powdered samples were consolidated into 6 mm diameter pellets (total mass ∼0.16 g) by pressing in a die and placed in an autoclave connected to Sievert's-type pressure−composition−temperature (PCT) apparatus (PCTPro-2000 system, Hy Energy LLC). The argon gas was removed from the autoclave by evacuation. Volume calibration was performed at room temperature for 90 minutes prior to each measurement. The thermal decomposition behavior of the Li_3AlH_6-3AB mixture was studied by continuously monitoring the pressure during heating of the sample from room temperature to the desired temperature with a rate of 1 °C per minute. During the isothermal dehydrogenation experiments, the mixture was being held at constant target temperature. The qualitative analysis of the gases released during the PCT measurements was carried out using the residual gas analyzer (RGA, quadrupolar mass spectrometer, RGAPro-2500, Hy-Energy LLC), connected to the PCT autoclave. For the solid-state NMR experiments, the mixture was held at selected temperatures, 40, 60, 80, and 100 °C, until the hydrogen release was no longer observed.

2.2. Solid-State NMR. The ^{11}B and ^{27}Al solid-state NMR experiments were performed at 9.4 T on a Chemagnetics Infinity 400 spectrometer, equipped with a 3.2 mm magic angle spinning (MAS) probe and operated at 400.0 MHz for ^{1}H, 128.3 MHz for ^{11}B, and 104.3 MHz for ^{27}Al. The samples were packed in MAS zirconia rotors in a glovebox under argon atmosphere and sealed with double O-ring caps to minimize the possibility of oxygen and moisture contamination. Several one- and two-dimensional (1D and 2D) experiments were carried out, including 1D ^{11}B and ^{27}Al direct polarization (DP) MAS, $^{27}Al\{^{1}H\}$ and $^{11}B\{^{1}H\}$ cross-polarization (CP) MAS, and ^{11}B multiple-quantum (MQ) MAS NMR. The DPMAS spectra of ^{27}Al and ^{11}B nuclei were acquired using a single pulse excitation with small flip angle of 15° for quantitative accuracy,[39] with or without ^{1}H decoupling using two-pulse phase-modulation (TPPM) method.[44] The MQMAS measurements used the Z-filter method with 200 kHz and ∼12 kHz for hard and soft pulses, respectively,[45] and continuous wave (CW) ^{1}H decoupling in both dimensions. Shearing and scaling of the MQMAS spectra were performed as described elsewhere, with the shifts along the MAS and isotropic dimensions denoted as δ and δ_{ISO}, respectively.[46,47] We note that the resonance frequencies in the MAS NMR spectra of quadrupolar nuclei depend on the chemical shifts (δ_{CS}) and quadrupole induced shifts (δ_{QIS}), and thus cannot be directly assigned based on the spectra taken in solutions. One of the benefits of MQMAS is that the precise values of δ_{CS}, δ_{QIS}, and the so-called second order quadrupolar effect (P_Q) can be directly determined from the analysis of a single 2D spectrum.[48−51]

All pertinent experimental conditions are given in figure captions using the following symbols: ν_{RF}^{X} denotes the magnitude of the radio frequency magnetic field applied to X spins, ν_R the MAS rate, Δt_1 the increment of t_1 during 2D acquisition, τ_{CP} the cross-polarization time, τ_{RD} the recycle delay, and NS the number of scans. The ^{11}B shifts were referenced to diethyl ether-boron trifluoride complex ($BF_3{\cdot}OEt_2$, $\delta\ ^{11}B = 0$ ppm), based on the measurement of a secondary reference (0.1 M aqueous solution of boric acid at 19.4 ppm).[52] The ^{27}Al shifts were referenced to 1.0 M aqueous solutions of $Al(NO_3)_3$ at $\delta\ ^{27}Al = 0$ ppm.

2.3. Theoretical Calculations. The chemical shift tensors and quadrupolar parameters were calculated by density functional theory (DFT) calculations using the ORCA program package.[53] The computations were performed for single molecule as well as crystalline models. For the single-molecule models, the geometries were first optimized at B3LYP level with 6-311G(d,p) basis set. An IGLO-II basis set[54,55] was then employed for the calculation of NMR parameters. The calculated shielding tensors were transformed to chemical shifts δ_{CS} relative to $BF_3{\cdot}OEt_2$.

3. RESULTS AND DISCUSSION

3.1. Dehydrogenation of the Li_3AlH_6-3AB Mixture. The kinetics of dehydrogenation of the Li_3AlH_6-3AB mixture was established based on the measurements of hydrogen release measured at several temperatures, similarly to the earlier studies (Figure 1a).[11,20] The activation energy for the dehydrogenation was estimated to be 110 (±8) kJ mol^{-1}, which is much lower than the values of 184 and 185 kJ mol^{-1} reported previously for pristine AB.[11,20] During all of the decompositions, no impurities such as borazine and diborane were observed using a mass spectrometer that was directly connected to the autoclave. The analysis was carried out after the temperature-controlled decomposition was completed, using residual gases collected in the autoclave. We note that potential difficulties in detecting transient gaseous impurities using mass spectrometry have been discussed recently by Borgschulte et al.;[56] however, our PCT-RGA setup did not allow for real-time monitoring of the gaseous decomposition products.

Reduction of the activation energy of AB dehydrogenation has been previously achieved using the mesoporous silica scaffolds or LiH.[11,20] In the case of mesoporous silica, the lowering in the activation energy was attributed to the defect sites arising from the templated nanostructural geometry of the AB in the scaffold and to the catalytic effect of the silanol groups within the silica materials.[11] In the LiH-AB mixture the activation energy was lowered to 76 kJ mol^{-1} and was associated with the formation of new chemical species,

dx.doi.org/10.1021/ic202368a | Inorg. Chem. 2012, 51, 4108−4115

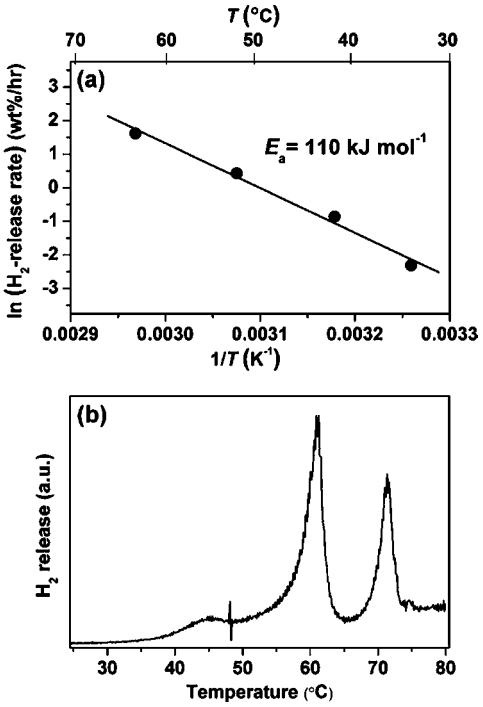

Figure 1. Dehydrogenation of the Li_3AlH_6-3AB mixture: (a) Arrhenius plot representing dehydrogenation kinetics, and (b) hydrogen desorption observed using the ramping rate of 1 °C/min. The accumulated hydrogen release as a function of temperature is shown in the Supporting Information (Figure SI-2).

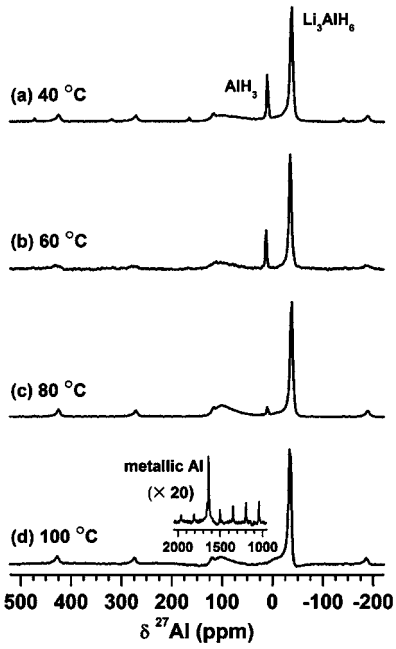

Figure 2. ^{27}Al DPMAS NMR spectra of the Li_3AlH_6-3AB mixture decomposed isothermally at various temperatures. The spectra were obtained using ν_R = 16 kHz, ν_{RF}^{Al} = 120 kHz, ν_{RF}^{H} = 64 kHz for TPPM ^{1}H decoupling, τ_{RD} = 30 s, and NS = 1200. The most intense peaks were normalized to constant height.

postulated to represent LiAB.[20] The hydrogen release taken by the temperature-controlled desorption with 1 °C/min ramping is shown in Figure 1b. The major hydrogen release from the mixture is observed at 60 and 72 °C. Since neither Li_3AlH_6 nor AB releases hydrogen in the pristine form at temperatures below 80 °C,[18,20,57] the release of hydrogen at 60 °C indicates that the dehydrogenation process from the Li_3AlH_6-3AB mixture involves a solid phase reaction between Li_3AlH_6 and AB. We also note that the dehydrogenation of pristine LiAB occurs around 92 °C under similar conditions (i.e., at 1 °C/min ramping).[19] In the present case, the decrease of the activation energy is not related to the formation of LiAB but is due to the formation of another intermediate, elucidated by the SSNMR measurements described below.

3.2. Solid-State NMR Experiments. The analysis of experimental and theoretical results is organized as follows. We first scrutinize the ^{27}Al and ^{11}B NMR results and propose the spectral assignments, in sections 3.2.1 and 3.2.2. These assignments will be further substantiated based on theoretical calculations described in section 3.3, and finally the dehydrogenation mechanism of the Li_3AlH_6-3AB mixture is given in section 3.4.

3.2.1. ^{27}Al NMR. Figure 2 shows the ^{27}Al DPMAS spectra of the Li_3AlH_6-3AB mixture treated at various temperatures, obtained with ^{1}H decoupling. The mixtures treated at 40 and 60 °C yielded two sharp signals at −38 ppm and 10 ppm and a broad one centered around 100 ppm, which are accompanied by weak spinning sidebands associated with the satellite transitions. In addition, the spectra of samples heated at 80 and 100 °C show a signal at 1630 ppm corresponding to metallic aluminum (shown in the inset in Figure 2d), whose relative contribution to the spectra increases concurrently with the decline of the signal at 10 ppm. We were unable to detect any ^{27}Al signal in the ^{27}Al{^{11}B} CPMAS experiment in the mixture treated at 40 °C.

The peak at −38 ppm is assigned to unreacted Li_3AlH_6, based on our earlier study of this compound,[38] and the ^{27}Al DPMAS spectrum of Li_3AlH_6 synthesized for the purpose of this work (see Figure SI-3 in the Supporting Information). The peak at 10 ppm most likely represents alane (AlH_3) formed within the Li_3AlH_6 matrix along with lithium hydride (LiH). This assignment is based on the NMR shift and the observed appearance of metallic Al upon further decomposition of this species at around 80 and 100 °C.[58−60] It is also consistent with the measured "build-up" of ^{27}Al polarization as a function of cross-polarization time τ_{CP} in the ^{27}Al{^{1}H} CPMAS experiment. Indeed, for each peak the time constant T_{IS} describing this process depends on the effective ^{1}H−^{27}Al magnetic dipole−dipole interaction, and thus the internuclear distance(s) and molecular mobility.[61−63] The T_{IS} value associated with the peak at 10 ppm was estimated at ∼70 μs, which confirms that it represents aluminum directly bound to hydrogen in a rigid lattice. Most likely, the elimination of LiH (via reaction with AB, see below) from Li_3AlH_6 forms domains of AlH_3, in which the octahedral units are strongly linked to each other via the shared hydrogen atoms. We note that the build-up of signal at −38 ppm was considerably slower, with T_{IS} of ∼230 μs. The weakening of dipolar ^{1}H−^{27}Al interactions in Li_3AlH_6 is attributed to internal mobility. Indeed, Li_3AlH_6 consists of isolated $[AlH_6]^{3-}$ octahedral units coordinated to Li^+ ions.[64] At room temperature, the $[AlH_6]^{3-}$ groups are expected to be mobile, most likely undergoing full isotropic reorientation.[65] The weak distributed peak around 100 ppm is assigned to disordered unreacted $LiAlH_4$,[38] which was retained during the preparation of Li_3AlH_6 via ball milling as verified by the ^{27}Al DPMAS measurement of the starting Li_3AlH_6 material (see Figure SI-3 in the Supporting Information).

dx.doi.org/10.1021/ic202368a | Inorg. Chem. 2012, 51, 4108−4115

3.2.2. ^{11}B NMR. Figure 3 shows the ^{11}B MAS NMR spectra of the corresponding samples, also measured with ^{1}H

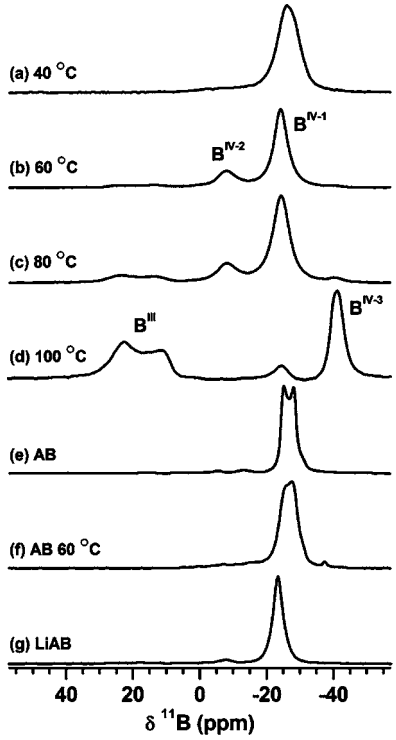

Figure 3. (a)−(d) ^{11}B DPMAS NMR spectra of the Li_3AlH_6-3AB mixture treated with various temperatures. Also shown are the spectra of pristine AB (e), pristine AB treated at 60 °C (f), and LiAB (g). The spectra were obtained using ν_R = 16 kHz, ν_{RF}^B = 120 kHz, ν_{RF}^H = 64 kHz for TPPM ^{1}H decoupling, τ_{RD} = 3 s, and NS = 64.

decoupling. In contrast to ^{27}Al NMR, the ^{11}B spectra of samples treated at 40 and 60 °C show different features. The mixture treated at 40 °C yielded a single broad signal whose position centered at −27 ppm corresponds to tetrahedrally coordinated boron species. In the sample held at 60 °C, this signal shifted to −24 ppm, and a new signal characteristic of tetrahedrally coordinated boron species appeared at −8 ppm. We denote these species as B^{IV-1} and B^{IV-2}, respectively. Two additional signals emerged, representing another tetrahedral species (−40 ppm, B^{IV-3}) and a MAS-averaged second order quadrupolar powder pattern typical of trigonally coordinated boron (10−30 ppm, B^{III}).[20,30,66] The intensities of these two peaks increased at 80 °C and dominated the spectrum of the sample decomposed at 100 °C, in which the signals due to B^{IV-1} and B^{IV-2} were considerably reduced and no longer observed, respectively. When the temperature was increased beyond 100 °C, the boron signal due to trigonal boron increased, while that of B^{IV-3} species decreased (spectra not shown).

The ^{11}B DPMAS spectra of isothermally treated Li_3AlH_6-3AB samples measured without ^{1}H decoupling are shown in Figure 4. The maximum amplitudes of signals due to B^{III} and B^{IV-3} are barely influenced by the ^{1}H coupling, while that of the B^{IV-1} is significantly decreased. The disappearance of signal at −8 ppm indicates that the B^{IV-2} site experiences the strongest dipolar broadening. The complementary results were obtained from the measurements of $^{11}B\{^{1}H\}$ cross-polarization (Table 1), performed in analogy to the $^{27}Al\{^{1}H\}$ CPMAS studies described above. Again, the fastest build-up of the CP signal for

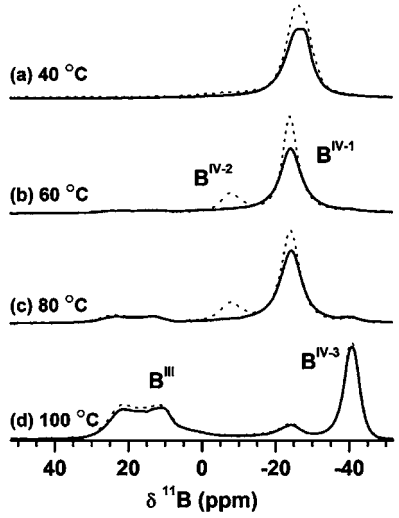

Figure 4. ^{1}H-coupled ^{11}B DPMAS NMR spectra of the Li_3AlH_6-3AB mixture treated at various temperatures. The spectra were obtained using ν_R = 16 kHz, ν_{RF}^B = 120 kHz, τ_{RD} = 3 s, and NS = 64. The dotted lines show the properly scaled ^{11}B DPMAS spectra measured with ^{1}H decoupling.

Table 1. Cross-Polarization Times T_{IS} (μs) for Individual Boron Sites in the Li_3AlH_6-3AB Mixture Treated at Various Temperatures

sample	B^{III}	B^{IV-2}	B^{IV-1}	B^{IV-3}
40 °C			135	
60 °C		19	134	
80 °C		18	151	1028
100 °C	63		161	1207

B^{IV-2} (T_{IS} < 20 μs) indicates a strong heteronuclear dipolar coupling, consistent with the existence of direct $^{1}H-^{11}B^{IV-2}$ bond(s) and lack of mobility on the NMR time scale ($\sim T_{IS}$). The B^{IV-3} site exhibits the least efficient CP transfer.

The MQMAS spectra of ^{11}B in Li_3AlH_6-3AB mixture treated at 60, 80, and 100 °C, as well as reference samples (LiAB and pristine AB) are shown in Figure 5. The line shape parameters δ_{CS}, δ_{QIS}, and P_Q obtained from the analysis of these spectra are listed in Table 2. The parameters associated with the trigonal site B^{III} are distributed because of structural disorder, with the P_Q values around 3.1 MHz.

The interpretation of boron spectra in Figures 3, 4, and 5 is as follows. The peak at −27 ppm in Figure 3a is dominated by unreacted AB. The resonances at −24 ppm in Figure 3b and c (denoted B^{IV-1}) also represent the $\equiv N-BH_3$ functionalities, which typically resonate in this spectral range.[66] Although similar resonances were observed by DPMAS in disordered AB and LiAB (Figure 3e and f), B^{IV-1} does not belong to these compounds. First, the MQMAS measurements revealed a clear distinction between the quadrupolar parameters in AB, LiAB, and B^{IV-1} (see Table 2). Second, the corresponding ^{27}Al spectra of the Li_3AlH_6-3AB mixtures (Figure 2a, b, and c) show that most of Li_3AlH_6 (~75%) remains unreacted in the samples; thus, the presence of pure LiAB or the previously observed LiAB·AB[30] cannot be confirmed at these temperatures. We also note that the disappearance of $\equiv N-BH_3$ species is not concurrent with any of the signals in the ^{27}Al spectra and the $^{11}B\rightarrow^{27}Al$ CP signals could not be detected, which suggests that the species in question is not affiliated with a compound

dx.doi.org/10.1021/ic202368a | Inorg. Chem. 2012, 51, 4108−4115

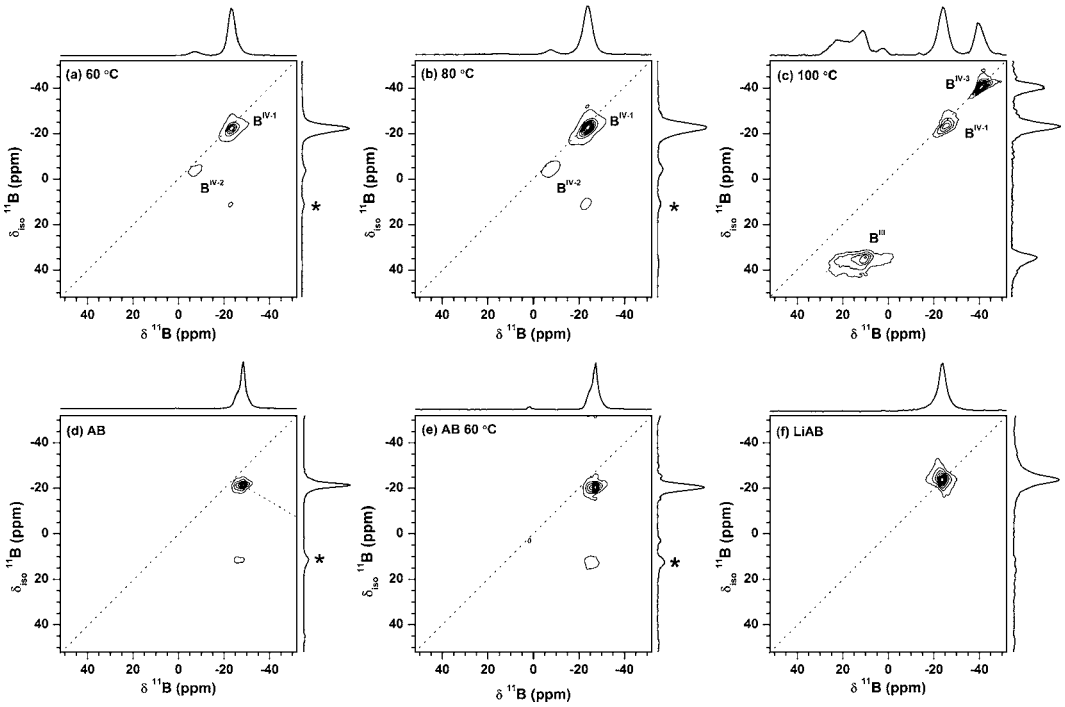

Figure 5. 2D ^{11}B MQMAS spectra of the Li_3AlH_6-3AB mixture treated at 60, 80, and 100 °C (a)−(c), and reference samples of pristine AB (d), pristine AB treated at 60 °C (e), and LiAB (f). The spectra were obtained using ν_R = 16 kHz, ν_{RF}^B = 200 kHz and 12 kHz for hard and soft (Z-filter) pulses respectively, and ν_{RF}^H = 64 kHz for CW ^{1}H decoupling. The data were acquired in 100 rows with Δt_1 = 20 μs, NS = 96 ((a)−(c)) or 24 ((d)−(f)) per row, and τ_{RD} = 3 s. The asterisks denote spinning sidebands.

Table 2. ^{11}B MQMAS Parameters Obtained for the Mixtures Treated at Various Temperatures and Reference Samples

sample	site	δ_{CS} (ppm)	δ_{QIS} (ppm)	P_Q (MHz)
60 °C	B^{IV-1}	−23.3	1.4	1.0
	B^{IV-2}	−5.9	2.6	1.3
80 °C	B^{IV-1}	−23.2	1.3	0.9
	B^{IV-2}	−5.8	2.4	1.3
100 °C[a]	B^{IV-1}	−24.0	1.2	0.9
	B^{IV-3}	−40.7	0.2	0.4
AB[b]		−23.9	3.7	1.6
LiAB		−24.1	0.5	0.5

[a]The B^{III} site appears to consist of multiple species based on its MQ projection, and the corresponding parameters are not estimated. [b]The same values were measured for pristine AB treated at 60 °C (Figure 5e).

containing aluminum. The T_{IS} value associated with this resonance (Table 1) and the effect of ^{1}H decoupling (Figure 4b and c) suggest that the ≡N−$\boldsymbol{B}$H$_3$ species exhibit restricted rotational motions about the N−B axis. We assign B^{IV-1} to ≡N−$\boldsymbol{B}$H$_3$ functionality in $(LiAB)_x(AB)_{1-x}$, an intermediate compound between AB and LiAB, and to the end groups in branched polyaminoboranes. These assignments will be further corroborated by theoretical calculations.

The B^{IV-2} resonance in Figure 3b and c (^{11}B peak at −8 ppm) can represent the branched (N−)$_3\boldsymbol{B}$H species or linear (N−)$_2\boldsymbol{B}$H$_2$ species in polyaminoboranes resulting from AB polymerization. Indeed, in the earlier studies of dehydrogenation of AB by solution NMR, the ^{11}B signals assigned to (N−)$_3\boldsymbol{B}$H and (N−)$_2\boldsymbol{B}$H$_2$ were observed around −5 ppm and between −10 and −13 ppm, respectively.[67] The 3 ppm difference between B^{IV-2} and (N−)$_3\boldsymbol{B}$H in solution matches exactly the δ_{QIS} shift obtained by ^{11}B MQMAS (Table 2). The presence of (N−)$_2\boldsymbol{B}$H$_2$ species could be invoked, assuming that lithium is responsible for the downfield shift of the B^{IV-2} resonance. However, our theoretical calculations below support the assignment of B^{IV-2} to the branched polyaminoboranes. The results in Figure 4 and Table 1 demonstrate the complete rigidity of these species at room temperature. Note that the polyaminoboranes were not detected during the decomposition of pristine AB. Indeed, the ^{11}B MQMAS spectrum of pristine AB treated at 60 °C showed one resonance at −26 ppm with δ_{CS} = −23.9 ppm and P_Q = 1.6 MHz (Figure 5e and Table 2).

The B^{IV-3} peak at −40 ppm, which is prominent in the sample held at 100 °C, is assigned to the [$\boldsymbol{B}$H$_4$]$^-$ anion. This assignment is consistent with the highest symmetry of this site measured by the MQMAS method (Table 2). The weak ^{1}H−$^{11}B^{IV-3}$ dipolar interaction (Table 1) is consistent with the rapid isotropic reorientation. A previous study has suggested that diammonia diborane ([$NH_3BH_2NH_3$]$^+$[BH_4]$^-$) is an intermediate species produced during thermal decomposition of AB.[18] However, the resonance due to [$NH_3\boldsymbol{B}H_2NH_3$]$^+$[$BH_4$]$^-$, known to occur around −15 ppm, was never found in our spectra, which further demonstrates that the dehydrogenation of AB in the presence of Li_3AlH_6 takes a different path than the thermolysis of pristine AB.

The B^{III} site has a rigid structure with trigonal symmetry, as evidenced by the characteristic powder pattern observed in the DPMAS and MQMAS spectra. The observed shift rules out the possibility of B^{III} being elemental boron, which would be expected near 5 ppm.[68] We assign B^{III} to the trigonal boron resulting from dehydrogenation of B^{IV-2}. Indeed, this site features a N=B double bond, and thus is trigonal, and has the same rigidity as B^{IV-2}. The lack of directly bound hydrogen results in slower CP transfer (T_{IS} = 63 μs, see Table 1), which now originates from the nearby NH_2 and NH_3 groups.

dx.doi.org/10.1021/ic202368a | Inorg. Chem. 2012, 51, 4108−4115

3.3. Theoretical Calculations. The δ_{CS} and P_Q values were calculated for boron sites as described in section 2.3. Since the NMR measurements did not detect any compounds containing both boron and aluminum, we focused on the linear and branched polyaminoboranes (Figure 6a and b), as well as single molecule and crystalline models of AB and LiAB (not shown), and crystalline model of LiAB·AB (Figure 7).

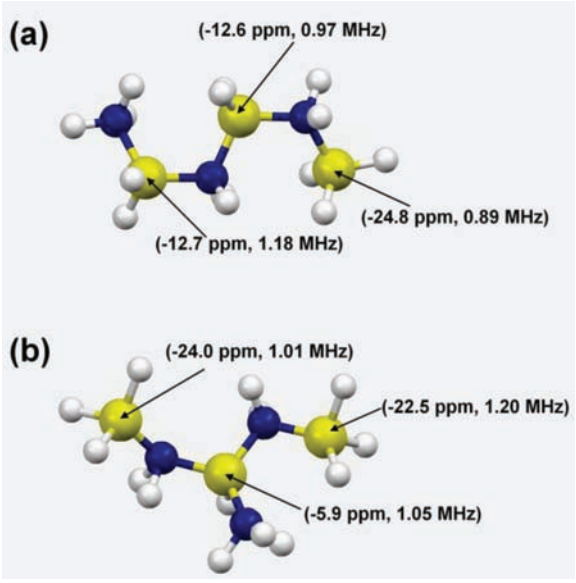

Figure 6. ^{11}B isotropic chemical shifts and second order quadrupolar effect (δ_{CS} ppm, P_Q MHz) calculated for the linear and branched polyaminoboranes. B, N, and H atoms are drawn in yellow, blue, and white, respectively.

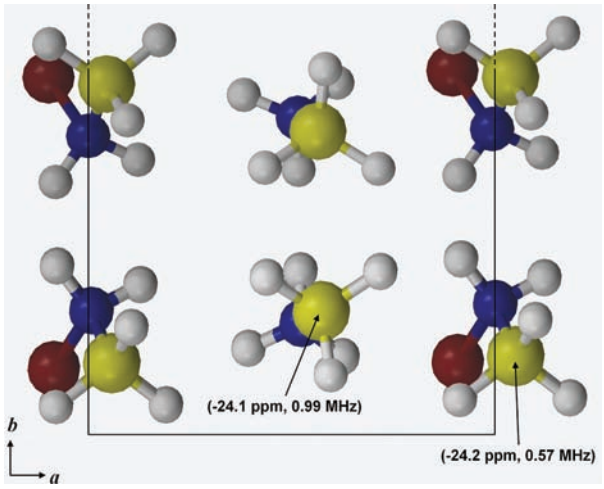

Figure 7. Schematic diagram of crystalline LiAB·AB and the resulting NMR parameters (δ_{CS} in ppm, P_Q in MHz). B, N, Li, and H atoms are shown in yellow, blue, red, and white, respectively. The calculations used an extended network of the basic units shown here.

For the branched $(N-)_3\boldsymbol{B}H$ species, the calculations yielded δ_{CS} = −5.9 ppm and P_Q = 1.05 MHz (Figure 6b), which is in good agreement with the values measured for the B^{IV-2} site (Table 2). The presence of linear $(N-)_2\boldsymbol{B}H_2$ functionality, which has been reported during dehydrogenation of pristine AB in both solid and liquid systems,[18,67] cannot be confirmed here, because the computed δ_{CS} values for such site (∼−13 ppm, Figure 6a) do not agree with the experimental values reported in Table 2. We also note that the parameters calculated for the terminal groups of polyaminoboranes ($\equiv N-\boldsymbol{B}H_3$) are similar to those of B^{IV-1}, which suggests that these groups indeed contribute to the peak observed around −24 ppm. The calculations performed for various lithium-containing cases indicated the downfield shift effect in both $(N-)_2\boldsymbol{B}H_2$ and $(N-)_3\boldsymbol{B}H$ sites. However no matches between theory and experiment were obtained to support such structures (see Supporting Information for details).

The calculations carried out for crystalline AB, LiAB, and LiAB·AB models (referred to as *c*-AB, *c*-LiAB, and *c*-LiAB·AB) were based on the existing crystallographic data.[30] For single molecules of AB and LiAB, the DTF computations were preceded by geometry optimizations. The crystalline and single molecule models yielded similar sets of parameters for both AB and LiAB (Table 3), which are also in good agreement with the experimental data, and support our earlier conclusion that the B^{IV-1} site cannot be assigned to AB or LiAB. Instead, we propose that it represents the previously discussed $\equiv N-\boldsymbol{B}H_3$ functionality in an intermediate compound between AB and LiAB, $(LiAB)_x(AB)_{1-x}$, as well as the end groups in branched polyaminoboranes. We estimated the δ_{CS} and P_Q values for boron in the intermediate species by using *c*-LiAB·AB as a model compound, which is composed of alternating layers of AB and LiAB (Figure 7).[30] The computed parameters for $LiNH_2\boldsymbol{B}H_3$ moiety in *c*-LiAB·AB (δ_{CS} = −24.1 ppm and P_Q = 0.57) are similar to those in *c*-LiAB (−22.7 and 0.59) or a single molecule of LiAB (−22.4 and 0.59), and agree well with the values measured for LiAB (Table 2). The values obtained for $NH_3\boldsymbol{B}H_3$ moiety in *c*-LiAB·AB do not agree as well with those calculated for *c*-AB and AB (Table 3) or measured experimentally.

Table 3. Theoretically Estimated Chemical Shifts (δ_{CS} in ppm) and Second Order Quadrupolar Effect (P_Q in MHz)

compound	site	δ_{CS}	P_Q
c-LiAB[35]	$LiNH_2\boldsymbol{B}H_3$	−22.7	0.59
c-AB[69]	$NH_3\boldsymbol{B}H_3$	−23.8	1.51
c-LiAB·AB[30]	$LiNH_2\boldsymbol{B}H_3$·AB	−24.1	0.57
	$LiAB{\cdot}NH_3\boldsymbol{B}H_3$	−24.2	0.99
LiAB[a]	$LiNH_2\boldsymbol{B}H_3$	−22.4	0.59
AB[a]	$NH_3\boldsymbol{B}H_3$	−21.3	1.45

[a]Single molecule model.

3.4. Dehydrogenation Mechanism of the Li_3AlH_6-3AB Mixture. The solid-state NMR experiments and theoretical calculations suggest that the presence of Li_3AlH_6 accelerates the formation of polyaminoborane species and improves the kinetics of AB dehydrogenation. The rapid hydrogen release from the mixture occurs at much lower temperature than from pristine LiAB,[41] which implies that the decrease of the activation energy is *not* due to the formation of LiAB in the present case. Indeed, "pure" LiAB is not found in the samples.

An earlier theoretical study has shown that the local density of states at the Fermi level (E_f-LDOS) at nitrogen in LiAB is higher than that in AB, which makes nitrogen in LiAB more reactive.[35] On the other hand, the E_f-LDOS at boron and hydrogen in LiAB (i.e., $LiNH_2\boldsymbol{B}H_3$) are lower than those in AB ($NH_3\boldsymbol{B}H_3$). These findings suggest that the polymerization between LiAB and AB, specifically nitrogen in LiAB and boron

dx.doi.org/10.1021/ic202368a | Inorg. Chem. 2012, 51, 4108−4115

in AB, is more preferred than between the same species, that is, LiAB-LiAB or AB-AB. Indeed, our results indicate the formation of $(LiAB)_x(AB)_{1-x}$ and subsequent polymerization in the Li_3AlH_6-3AB mixture treated at temperatures as low as 50 °C, which lowers the activation energy of dehydrogenation of the mixture. A similar result has been reported in the study of dehydrogenation of LiAB·AB, which released hydrogen at lower temperature (80 °C) than pristine LiAB (90 °C) under 2 °C/min ramping condition.[30] Both our results and the earlier study demonstrate that the improvement of dehydrogenation kinetics is due to the coexistence of AB and LiAB at a molecular level.

The reaction mechanism below 80 °C can be summarized as follows. First, a part of AB is transformed into LiAB yielding $(LiAB)_x(AB)_{1-x}$

$$x/3Li_3AlH_6 + NH_3BH_3 \rightarrow (LiNH_2BH_3)_x(NH_3BH_3)_{1-x} + x/3AlH_3 + xH_2 \quad (1)$$

Subsequently, LiAB reacts with the AB,

$$NH_3BH_3 + LiNH_2BH_3 \rightarrow NH_3BH_2{-}NH_2BH_3 + LiH \quad (2)$$

which leads to the formation of branched polyaminoborane species

$$NH_3BH_2{-}NH_2BH_3 + LiNH_2BH_3 \rightarrow NH_3BH(NH_2BH_3)_2 + LiH \quad (3)$$

The LiH formed in the polymerization process reacts with NH_3BH_3 to yield $LiNH_2BH_3$ (eq 1).

The growth of linear polyaminoborane structures has not been detected. We note that the formation of boron−boron bonds has been recently suggested in the theoretical and experimental study of the decomposition of pristine LiAB by Wolstenholme et al.,[70] which raises the possibility that the same reaction could occur in the Li_3AlH_6-3AB mixture. We examined this scenario by carrying out a DFT calculation of $-BH_2-N\equiv$ functionalities in $NH_3BH(-BH_2NH_3)_2$. Such functionalities would exist in any plausible structures involving the B−B bond. The computed chemical shift of boron in this structure is around −15 ppm (see Supporting Information). We have not detected ^{11}B signals in the vicinity of −15 ppm in any of our samples, which suggests that the formation of B−N bond is dominant in our system.

When the temperature is increased beyond 80 °C, additional hydrogen is released resulting in forming B=N double bonds[71,72]

$$NH_3BH(NH_2BH_3)_2 \rightarrow NH_3B(=NHBH_3)(-NH_2BH_3) + H_2 \quad (4)$$

and the B^{III} sites detected by SSNMR.

We note that the proposed mechanism does not involve the BH_4 species, whose formation was clearly indicated by the ^{11}B spectrum of the Li_3AlH_6-3AB mixture treated at 100 °C but most likely results from decomposition of AB without the assistance of Li_3ALH_6.

4. CONCLUSION

In summary, solid-state NMR measurements and theoretical calculations provided invaluable insights into the dehydrogenation mechanism of the Li_3AlH_6-3AB mixture. The key reactions involved in this process were identified by a suite of 1D and 2D NMR measurements, which provided coherent information about ^{27}Al and ^{11}B functionalities in samples treated at various temperatures. The DFT calculations were used to further refine the understanding of these functionalities, in cases when the spectroscopic information alone could not provide definite identification. These results revealed that the partial transformation of AB to LiAB yields the $(LiAB)_x(AB)_{1-x}$ intermediate, which promotes the polymerization between AB and LiAB, and results in the lower activation energy for the dehydrogenation. The detailed reaction mechanism, in particular the role of lithium revealed in this study, open up opportunities for exploring new classes of hydrogen storage materials (both pure compounds and mixtures) and strategies for their utilization.

■ ASSOCIATED CONTENT

Supporting Information

The X-ray diffraction data of prepared Li_3AlH_6 and LiAB, the accumulated hydrogen release from the Li_3AlH_6-3AB mixture as a function of temperature, the ^{27}Al DPMAS measurement of the starting Li_3AlH_6 material, the estimations of chemical shifts and second order quadrupolar effect of Li-containing polyaminoborane. This material is available free of charge via the Internet at http://pubs.acs.org.

■ AUTHOR INFORMATION

Corresponding Author

*Phone: (515)294-2017. E-mail:mpruski@iastate.edu.

Notes

The authors declare no competing financial interest.

■ ACKNOWLEDGMENTS

This research was supported at the Ames Laboratory by the U.S. Department of Energy, Office of Basic Energy Sciences, Division of Materials Sciences and Engineering. Ames Laboratory is operated for the U.S. Department of Energy by Iowa State University under Contract No. DE-AC02-07CH11358.

■ REFERENCES

(1) Hamilton, C. W.; Baker, R. T.; Staubitz, A.; Manners, I. *Chem. Soc. Rev.* **2009**, *38*, 279−293.
(2) Vajo, J. J.; Olson, G. L. *Scr. Mater.* **2007**, *56*, 829−834.
(3) Ogden, J. M. *Annu. Rev. Energy Env.* **1999**, *24*, 227−279.
(4) Hydrogen Storage: Current Technology. Hydrogen, fuel cells and infrastructure technologies program; http://www1.eere.energy.gov/hydrogenandfuelcells/storage/current_technology.html.
(5) Thomas, K. M. *Catal. Today* **2007**, *120*, 389−398.
(6) Sandrock, G. *J. Alloys Compd.* **1999**, *293*, 877−888.
(7) Schüth, F.; Bogdanovic, B.; Felderhoff, M. *Chem. Commun.* **2004**, 2249−2258.
(8) Orimo, S. I.; Nakamori, Y.; Eliseo, J. R.; Zuttel, A.; Jensen, C. M. *Chem. Rev.* **2007**, *107*, 4111−4132.
(9) Chen, P.; Xiong, Z. T.; Luo, J. Z.; Lin, J. Y.; Tan, K. L. *Nature* **2002**, *420*, 302−304.
(10) Zuttel, A. *Mater. Today* **2003**, *6*, 24−33.
(11) Gutowska, A.; Li, L. Y.; Shin, Y. S.; Wang, C. M. M.; Li, X. H. S.; Linehan, J. C.; Smith, R. S.; Kay, B. D.; Schmid, B.; Shaw, W.; Gutowski, M.; Autrey, T. *Angew. Chem., Int. Ed.* **2005**, *44*, 3578−3582.
(12) Denney, M. C.; Pons, V.; Hebden, T. J.; Heinekey, D. M.; Goldberg, K. I. *J. Am. Chem. Soc.* **2006**, *128*, 12048−12049.

(13) Keaton, R. J.; Blacquiere, J. M.; Baker, R. T. *J. Am. Chem. Soc.* **2007**, *129*, 1844−1845.
(14) Yan, J. M.; Zhang, X. B.; Han, S.; Shioyama, H.; Xu, Q. *Angew. Chem., Int. Ed.* **2008**, *47*, 2287−2289.
(15) Chandra, M.; Xu, Q. *J. Power Sources* **2006**, *156*, 190−194.
(16) Stephens, F. H.; Pons, V.; Baker, R. T. *Dalton Trans.* **2007**, 2613−2626.
(17) Cheng, F. Y.; Ma, H.; Li, Y. M.; Chen, J. *Inorg. Chem.* **2007**, *46*, 788−794.
(18) Stowe, A. C.; Shaw, W. J.; Linehan, J. C.; Schmid, B.; Autrey, T. *Phys. Chem. Chem. Phys.* **2007**, *9*, 1831−1836.
(19) Xiong, Z. T.; Yong, C. K.; Wu, G. T.; Chen, P.; Shaw, W.; Karkamkar, A.; Autrey, T.; Jones, M. O.; Johnson, S. R.; Edwards, P. P.; David, W. I. F. *Nat. Mater.* **2008**, *7*, 138−141.
(20) Kang, X. D.; Fang, Z. Z.; Kong, L. Y.; Cheng, H. M.; Yao, X. D.; Lu, G. Q.; Wang, P. *Adv. Mater.* **2008**, *20*, 2756−2759.
(21) Xiong, Z. T.; Chua, Y. S.; Wu, G. T.; Xu, W. L.; Chen, P.; Shaw, W.; Karkamkar, A.; Linehan, J.; Smurthwaite, T.; Autrey, T. *Chem. Commun.* **2008**, 5595−5597.
(22) Heldebrant, D. J.; Karkamkar, A.; Hess, N. J.; Bowden, M.; Rassat, S.; Zheng, F.; Rappe, K.; Autrey, T. *Chem. Mater.* **2008**, *20*, 5332−5336.
(23) Bowden, M.; Autrey, T.; Brown, I.; Ryan, M. *Curr. Appl. Phys.* **2008**, *8*, 498−500.
(24) Lee, T. B.; McKee, M. L. *Inorg. Chem.* **2009**, *48*, 7564−7575.
(25) He, T.; Xiong, Z. T.; Wu, G. T.; Chu, H. L.; Wu, C. Z.; Zhang, T.; Chen, P. *Chem. Mater.* **2009**, *21*, 2315−2318.
(26) Kalidindi, S. B.; Joseph, J.; Jagirdar, B. R. *Energy Env. Sci.* **2009**, *2*, 1274−1276.
(27) Kang, X. D.; Ma, L. P.; Fang, Z. Z.; Gao, L. L.; Luo, J. H.; Wang, S. C.; Wang, P. *Phys. Chem. Chem. Phys.* **2009**, *11*, 2507−2513.
(28) Luo, J. H.; Kang, X. D.; Wang, P. *ChemPhysChem* **2010**, *11*, 2152−2157.
(29) Wu, C. Z.; Wu, G. T.; Xiong, Z. T.; David, W. I. F.; Ryan, K. R.; Jones, M. O.; Edwards, P. P.; Chu, H. L.; Chen, P. *Inorg. Chem.* **2010**, *49*, 4319−4323.
(30) Wu, C.; Wu, G.; Xiong, Z.; Han, X.; Chu, H.; He, T.; Chen, P. *Chem. Mater.* **2010**, *22*, 3−5.
(31) Xiong, Z. T.; Chua, Y. S.; Wu, G. T.; Wang, L.; Wong, M. W.; Kam, Z. M.; Autrey, T.; Kemmitt, T.; Chen, P. *Dalton Trans.* **2010**, *39*, 720−722.
(32) Sutton, A. D.; Burrell, A. K.; Dixon, D. A.; Garner, E. B.; Gordon, J. C.; Nakagawa, T.; Ott, K. C.; Robinson, P.; Vasiliu, M. *Science* **2011**, *331*, 1426−1429.
(33) DOE Hydrogen Program Review, http://www.hydrogen.energy.gov/pdfs/review07/st_27_sneddon.pdf.
(34) Neiner, D.; Karkamkar, A.; Linehan, J. C.; Arey, B.; Autrey, T.; Kauzlarich, S. M. *J. Phys. Chem. C* **2009**, *113*, 1098−1103.
(35) Wu, H.; Zhou, W.; Yildirim, T. *J. Am. Chem. Soc.* **2008**, *130*, 14834−14839.
(36) Zhang, Q. A.; Tang, C. X.; Fang, C. H.; Fang, F.; Sun, D.; Ouyang, L. Z.; Zhu, M. *J. Phys. Chem. C* **2010**, *114*, 1709−1714.
(37) Graham, K. R.; Kemmitt, T.; Bowden, M. E. *Energy Env. Sci.* **2009**, *2*, 706−710.
(38) Balema, V. P.; Wiench, J. W.; Dennis, K. W.; Pruski, M.; Pecharsky, V. K. *J. Alloys Compd.* **2001**, *329*, 108−114.
(39) Wiench, J. W.; Balema, V. P.; Pecharsky, V. K.; Pruski, M. *J. Solid State Chem.* **2004**, *177*, 648−653.
(40) Dolotko, O.; Kobayashi, T.; Wiench, J. W.; Pruski, M.; Pecharsky, V. *Int. J. Hydrogen Energy* **2011**, *36*, 10626−10634.
(41) Luedtke, A. T.; Autrey, T. *Inorg. Chem.* **2010**, *49*, 3905−3910.
(42) *NMR Crystallography*; Harris, R. K.; Wasylishen, R. E.; Duer, M. J., Eds.; Wiley: Chichester, U.K., 2009.
(43) Dolotko, O.; Zhang, H. Q.; Ugurlu, O.; Wiench, J. W.; Pruski, M.; Chumbley, L. S.; Pecharsky, V. *Acta Mater.* **2007**, *55*, 3121−3130.
(44) Bennett, A. E.; Rienstra, C. M.; Auger, M.; Lakshmi, K. V.; Griffin, R. G. *J. Chem. Phys.* **1995**, *103*, 6951−6958.
(45) Amoureux, J. P.; Fernandez, C.; Steuernagel, S. *J. Magn. Reson. A* **1996**, *123*, 116−118.
(46) Massiot, D.; Touzo, B.; Trumeau, D.; Coutures, J. P.; Virlet, J.; Florian, P.; Grandinetti, P. J. *Solid State Nucl. Magn. Reson.* **1996**, *6*, 73−83.
(47) Amoureux, J. P.; Fernandez, C. *Solid State Nucl. Magn. Reson.* **1998**, *10*, 211−223.
(48) Frydman, L.; Harwood, J. S. *J. Am. Chem. Soc.* **1995**, *117*, 5367−5368.
(49) Medek, A.; Harwood, J. S.; Frydman, L. *J. Am. Chem. Soc.* **1995**, *117*, 12779−12787.
(50) Lacassagne, V.; Florian, P.; Montouillout, V.; Gervais, C.; Babonneau, F.; Massiot, D. *Magn. Reson. Chem.* **1998**, *36*, 956−959.
(51) Amoureux, J. P.; Pruski, M. In *Encyclopedia of Nuclear Magnetic Resonance*; Grant, D. M., Harris, R. K., Eds.; John Wiley & Sons: Chichester, U.K., 2002; Vol. *9*, pp 226−251.
(52) Matsuo, H.; Miyazaki, Y.; Takemura, H.; Matsuoka, S.; Sakashita, H.; Yoshimura, K. *Polyhedron* **2004**, *23*, 955−961.
(53) Neese, F. *ORCA-An Ab initio, DFT and Semiempirical Electronic Structure Package*, Ver. 2.8.0.; 2011;
(54) Kutzelnigg, W.; Fleischer, U.; Schindler, M.; Springer-Verlag: Heidelberg, Germany, 1990; Vol. *23*.
(55) Huzinaga, S. *J. Chem. Phys.* **1965**, *42*, 1293−1302.
(56) Borgschulte, A.; Callini, E.; Probst, B.; Jain, A.; Kato, S.; Friedrichs, O.; Remhof, A.; Bielmann, M.; Ramirez-Cuesta, A. J.; Zuttel, A. *J. Phys. Chem. C* **2011**, *115*, 17220−17226.
(57) Liu, S. S.; Sun, L. X.; Zhang, J. A.; Zhang, Y.; Xu, F.; Xing, Y. H.; Li, F.; Zhao, J. J.; Du, Y.; Hu, W. Y.; Deng, H. Q. *Int. J. Hydrogen Energy* **2010**, *35*, 8122−8129.
(58) Hwang, S. J.; Bowman, R. C.; Graetz, J.; Reilly, J. J.; Langley, W.; Jensen, C. M. *J. Alloys Compd.* **2007**, *446*, 290−295.
(59) Graetz, J.; Reilly, J. J. *J. Phys. Chem. B* **2005**, *109*, 22181−22185.
(60) Graetz, J.; Reilly, J. J.; Kulleck, J. G.; Bowman, R. C. *J. Alloys Compd.* **2007**, *446*, 271−275.
(61) Mehring, M. *Principles of High Resolution NMR in Solids*, 2nd ed.; Spinger-Verlag: New York, 1983.
(62) Keeler, C.; Maciel, G. E. *Anal. Chem.* **2003**, *75*, 2421−2432.
(63) Amoureux, J. P.; Pruski, M. *Mol. Phys.* **2002**, *100*, 1595−1613.
(64) Sato, T.; Ramires-Cuesta, A. J.; Ikeda, K.; Orimo, S. I. *Inorg. Chem.* **2011**, *50*, 8007−8011.
(65) Majer, G.; Stanik, E.; Banuet, L. E. V.; Grinberg, F.; Kircher, O.; Fichtner, M. *J. Alloys Compd.* **2005**, *404*, 738−742.
(66) Gervais, C.; Babonneau, F. *J. Organomet. Chem.* **2002**, *657*, 75−82.
(67) Bluhm, M. E.; Bradley, M. G.; Butterick, R.; Kusari, U.; Sneddon, L. G. *J. Am. Chem. Soc.* **2006**, *128*, 7748−7749.
(68) Zhao, J.-C.; Knight, D. A.; Brown, G. M.; Kim, C.; Hwang, S.-J.; Reiter, J. W.; Bowman, R. C. Jr.; Zan, J. A.; Kulleck, J. G. *J. Phys. Chem. C* **2009**, *113*, 2−11.
(69) Yang, J. B.; Lamsal, J.; Cai, Q.; James, W. J.; Yelon, W. B. *Appl. Phys. Lett.* **2008**, *92*, 091916.
(70) Wolstenholme, D. J.; Titah, J. T.; Che, F. N.; Traboulsee, K. T.; Flogeras, J.; McGrady, G. S. *J. Am. Chem. Soc.* **2011**, *133*, 16598−16604.
(71) Dixon, D. A.; Gutowski, M. *J. Phys. Chem. A* **2005**, *109*, 5129−5135.
(72) Staubitz, A.; Besora, M.; Harvey, J. N.; Manners, I. *Inorg. Chem.* **2008**, *47*, 5910−5918.